Tire Force Estimation of Dynamic Wheeled Mobile Robots using Tire-Model Based Constrained Kalman Filtering

Sang-Yun Jeon, Rakjoon Chung, and Dongjun Lee

Abstract— **We propose a novel real-time algorithm to estimate the full three-dimensional individual tire forces (i.e., vertical, longitudinal as well as lateral) of a car-like rearwheel-driven four wheel wheeled mobile robots equipped with onboard navigation sensors and wheel encoders. The key enabling idea for this is to utilize the tire model (i.e., the magic formula) in a feedback manner on the framework of the constrained Kalman filtering to render the tire force estimation: 1) more accurate as compared to the typical tire force estimation techniques neglecting the tire-road interaction; and 2) more robust as compared to the results adopting the tire model, yet, only in an open-loop manner. Our proposed algorithm, while performing this full tire force onboard/real-time estimation, also provides the estimation of: 1) tire-road friction coefficient; and 2) torque inputs of the rear left and right wheels, which are connected via differential gear. Simulations with CarSim and outdoor experiments are performed to validate the proposed estimation algorithm.**

I. INTRODUCTION

Recently, there has been increasing interest in high-speed or dynamic WMRs (wheeled mobile robots), since it can not only significantly enhance the operation speed of the conventionally slow-speed/kinematic WMRs (e.g., [1], [2]), but also can allow us to attain some interesting behaviors impossible to those slow-speed/kinematic WMRs (e.g., [3]–[5]). This dynamic WMR can also serve as a platform to investigate many important aspects of autonomous driving and to develop solutions for that as well in a safer and more affordable manner (e.g., driving in friction-limit [6], turnover prevention [7], rough-terrain dynamic driving [8], etc.). To attain such high-speed operations of this dynamic WMR, it is then important to precisely estimate the individual tire-road interaction forces to monitor them not to exceed certain threshold to prevent (often unsafe) slippage (e.g., [3], [6]) or to control them in certain way to intentionally trigger/maintain the slippage (e.g., [4], [5]). This should also be done by using only onboard sensors and in realtime for their real-world adoption. Many strong techniques and results have been proposed for this onbaord/real-time tire force estimation and also its related tire-road friction estimation [9]–[14]. However, the majority of them, instead of relying on some accurate nonlinear tire models (e.g., Pacejka model [15], Doughoff model [16], brush model [16]), which are known to properly capture the (crucial) effects of the slip on the tire-road force, rather compute the sums of some individual tire forces (e.g., total front tire force via bicycle models: e.g., [13]) and split them to individual tire force rather in an ad-hoc manner (e.g., proportional to vertical tire force [9]) while neglecting such important tire-road interaction model.

Particularly difficult to estimate is the lateral tire force, since, in contrast to the case of longitudinal tire force, which can be rather more straightforwardly determined for each wheel by using their respective wheel spin dynamics (with its acceleration sensing via, e.g., encoders) with the known (or estimated) wheel torque input, the lateral tire force does not allow us to utilize such wheel-level dynamics as the wheel-spin dynamics. This lateral tire force, however, is crucial to attain such behaviors as drifting [3]–[5] or to prevent side-way slip during dynamics driving [6]. Only few results have proposed techniques to estimate this lateral tire force dynamics (e.g., [9]–[11]), yet, again, the tire-road interaction model is neglected and some ad-hoc measures are used to determine the (individual) lateral tire force (e.g., [9]). The tire-models are adopted in [10], [11] to estimate this lateral tire force, which, however, are fully exposed to the uncertainty of their adopted tire (Doughoff or brush) model, with no such feedback correction loop to reduce the uncertainty effect as done in typical state estimation with sensor feedback.

In this paper, we propose a novel real-time algorithm to estimate the full three-dimensional individual tire forces (i.e., vertical, longitudinal as well as lateral) of a car-like rear wheel-driven four wheel WMR with rear-wheel differential and also equipped only with typical onboard sensors (i.e., wheel encoders, INS (inertial navigation system) or IMU (inertial measurement unit), and GNSS (global navigation satellite system)). The key enabling idea for this is to utilize the tire model (i.e., the magic formula) in a feedback manner on the framework of the constrained Kalman filtering [17], so that the tire force estimation can be: 1) more accurate as compared to, e.g., those tire-model-less techniques [9], [12]; and also 2) more robust as compared to, e.g., the one adopting the tire-model, yet, only in an open-loop manner [10], [11]. Our proposed algorithm, while performing this full tire force onboard/real-time estimation, also provides the estimation of: 1) tire-road friction coefficient; and 2) torque inputs of the rear left and right wheels, which are connected via differential gear.

More precisely, our proposed estimation algorithm consists of the following three steps: 1) tire force estimation

Research supported in part by the Industrial Convergence Core Technology Development Program (10063172) funded by MOTIE, Korea; the Bio-Mimetic Robot Research Center (UD130070ID), DAPA/ADD, Korea; and the Urban Data Science Lab Project (UDSL 0660-20170004), Seoul Digital Foundation, Seoul Metropolitan Government, Korea.

The authors are with the Department of Mechanical & Aerospace Engineering, Seoul National University and IAMD, Seoul, 151-744, Republic of Korea. Corresponding author: D. J. Lee (djlee@snu.ac.kr).

Kalman filter (TF-KF), which estimates the full (i.e., vertical, longitudinal and lateral) tire forces of each wheel and the rear left and right wheel torque inputs using the information (i.e., output) of the body and wheel-spin accelerations, the vertical tire forces (computed via the effective mass approach [9], [18]), and the lateral tire forces (computed via the linearized tire model); 2) friction coefficient estimation, which estimates friction coefficient using the Bayesian hypothesis selection algorithm [12] by using the tire forces priorly estimated by the TF-KF; and 3) tire model constrained Kalman filter, which optimally projects the estimated longitudinal and lateral tire forces onto the accurate tire model with the uncertainties of the estimated tire forces and the tire model taken into account on the framework of the constrained Kalman filtering (CKF) [17], while its results is fed back to the TF-KF, completing the feedback-loop, thereby, substantially improving robustness and accuracy of the estimation (see Sec. IV). We call our estimation framework TFF-CKF (tire force and friction coefficient constrained Kalman filtering). This TFF-CKF also stands upon the standard state estimation federated Kalman filter (FKF) [19], [20], which estimate the position, velocity, attitude and the biases of the IMU.

The organization of this paper is as follows. Section II briefly describes the system and implemented sensors. The proposed TFF-CKF is provided with its observability analysis in Section III. In Section IV, the proposed TFF-CKF are verified with the CarSim based simulation and outdoor experiments. Finally, the conclusion of the paper is drawn in Section V.

II. SYSTEM MODEL AND SENSOR CONFIGURATION

In this section, we provide the system model and sensor configuration of WMR which are used for the proposed tire force and friction coefficient estimation algorithm utilizing the constrained KF (TFF-CKF). The WMR considered in this paper is the most common rearwheel-driven (RWD) vehicle which has one actuator and a differential gear for the rear wheels. The front wheels do not have any actuator and can be steered using a steering wheel. Onboard sensors (e.g., an INS, an encoder for each wheel, and a GNSS receiver) are implemented on the WMR to estimate the state, tire forces, and friction coefficient. The INS, encoder, and GNSS receiver are installed at the center of gravity (CoG) of the WMR, the rotation center of each front wheel, and the top of the WMR, respectively. See Fig. 1 for the sensor configuration.

To formulate the dynamic equations of the WMR, the global and body frames are defined. The global frame $\{\mathcal{G}\}$ has the origin at the center of the Earth, and the body frame $\{\mathcal{B}\}$ has the origin at the CoG of the WMR as shown in Fig. 1. In $\{\mathcal{B}\}$, the tire forces of the wheels are defined as depicted in Fig. 1. The index $i \in A\,(=[\text{lf, rf, lr, rr}])$ is defined to indicate each wheel of the WMR, where lf, rf, lr, and rr represent the left-front, right-front, left-rear, and right-rear wheels, respectively.

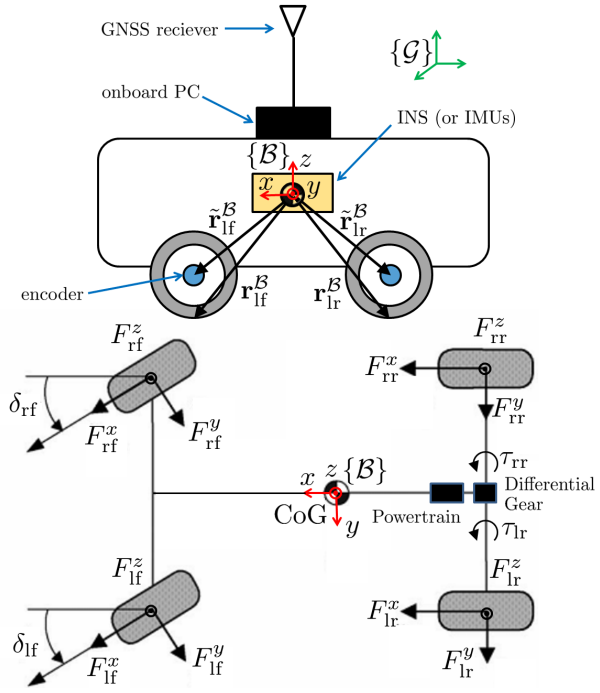

Fig. 1: System and sensor configuration of a RWD WMR.

Using the definitions of the frames and tire forces, the 6-degree of freedom (DOF) dynamic equations of motion are expressed as

$$\mathcal{I}_{tot}\dot{\boldsymbol{\Omega}}^{\mathcal{B}} + \boldsymbol{\Omega}^{\mathcal{B}} \times \mathcal{I}_{tot}\boldsymbol{\Omega}^{\mathcal{B}} = \sum_{i\in A} \mathbf{r}_i^{\mathcal{B}} \times \mathbf{F}_i^{\mathcal{B}} \quad (1)$$

$$m_{tot}(\mathbf{a}^{\mathcal{B}} + \mathbf{g}^{\mathcal{B}} + \boldsymbol{\Omega}^{\mathcal{B}} \times \mathbf{V}^{\mathcal{B}}) = \sum_{i\in A} \mathbf{F}_i^{\mathcal{B}}, \quad (2)$$

where $\mathcal{I}_{tot} \in \Re^3$ and m_{tot} are, respectively, the inertial matrix and the mass of the WMR. The vector $\mathbf{F}_i^{\mathcal{B}} \in \Re^3$ is the three-dimensional tire force vector of the i wheel in $\{\mathcal{B}\}$, and $\mathbf{g}^{\mathcal{B}}$ is the gravity vector in $\{\mathcal{B}\}$. The vector $\mathbf{r}_i^{\mathcal{B}} = [r_i^x \; r_i^y \; r_i^z]^{\mathrm{T}} \in \Re^3$ is the relative position vector from the CoG of the WMR to the contact point of the road and the i wheel as shown in Fig. 1. The angular acceleration of the WMR $\dot{\boldsymbol{\Omega}}^{\mathcal{B}} \in \Re^3$ can be obtained by differentiating the gyroscope measurements [21], and $\mathbf{a}^{\mathcal{B}} \in \Re^3$ represents the accelerometer measurements. The quantity $\mathbf{V}^{\mathcal{B}}$ is the velocity of the WMR in $\{\mathcal{B}\}$ which can be obtained using the onboard sensors. The 6-DOF dynamic equations can be used as the measurements to estimate the tire forces, yet the signal to noise ratio (SNR) of the differentiated gyroscope measurements are too small to be used in practice. Therefore, the proposed TFF-CKF do not use the rotation dynamic equation which is expressed in (1). The tire forces are observable using the proposed TFF-CKF without the rotation dynamics in (1) as shown in Section IV. Yet, using the rotation dynamics is one of our future work to increase the accuracy. The proposed TFF-CKF also uses the wheel dynamic equation as the following.

$$\mathcal{I}_{wheel}\dot{\Omega}_{wheel,i} = \tau_i - r_{eff} \cdot F_i^x, \quad (3)$$

where $\mathcal{I}_{wheel}$, $\dot{\Omega}_{wheel,i}$, τ_i, and F_i^x are, respectively, the

moment of inertia, differentiated angular velocity measurement, input torque, and longitudinal tire force of the i wheel. The effective radius of the wheels is notated with r_{eff}. The encoder measurement $\Omega_{wheel,i}$ should be differentiated to obtain the differentiated angular velocity. Typically, the SNR of $\Omega_{wheel,i}$ is high enough to be used in practice, because the magnitude of the measurements from an encoder is much greater than the magnitude of the noise. The details of the proposed TFF-CKF using the above dynamic equations are provided in Section III.

For the better performance, the accelerometer and gyroscope measurements are compensated with the estimated IMU biases using the federated Kalman filter (FKF) [19], [20]. As it is shown in Fig. 2, the FKF provides the estimated state $\hat{\mathbf{x}}_m = [\hat{\mathbf{P}}^{\mathcal{G}}\ \hat{\mathbf{V}}^{\mathcal{G}}\ \hat{\mathbf{\Theta}}^{\mathcal{G}}\ \hat{\mathbf{b}}_a\ \hat{\mathbf{b}}_\Omega]^{\mathrm{T}}$ and the estimated state error covariance $\hat{\mathbf{\Sigma}}_m$ to the proposed TFF-CKF using the onboard sensors, where $\hat{\mathbf{P}}^{\mathcal{G}}$, $\hat{\mathbf{V}}^{\mathcal{G}}$, $\hat{\mathbf{\Theta}}^{\mathcal{G}}$, $\hat{\mathbf{b}}_a$, and $\hat{\mathbf{b}}_\Omega$ are, respectively, the estimated position, velocity, attitude, accelerometer bias, and gyroscope bias. Please see [19], [20] for the details of the FKF.

III. TIRE FORCE AND FRICTION COEFFICIENT ESTIMATION ALGORITHM

The proposed TFF-CKF has three steps as shown in Fig. 2. The first step is estimating the tire forces (e.g., the longitudinal, lateral, and vertical tire forces) using the proposed tire force estimation algorithm using the KF (TF-KF) with the estimated state, dynamic equations, and onboard sensor measurements. While using the existing algorithms to estimate the tire forces, the vertical tire forces are observable using the effective mass approach as proposed and verified empirically in [9], [18]. However, the lateral tire force of each wheel is unobservable as highlighted in [9] and [15]. To estimate all the tire forces of each wheel, we assumed that the lateral tire forces can be estimated using the linearized tire model in this step. The details of the linearized tire model is described in III-A. The estimated tire forces using the proposed TF-KF contains errors due to the effective mass approach and the linearized tire model. Therefore, we employed the constrained KF (CKF) using the tire model (magic formula) [15], [16] to improve the estimation accuracy of the longitudinal and lateral tire forces. The friction coefficient is essential to extract the longitudinal and lateral tire forces from the tire model, so the proposed TFF-CKF estimates the friction coefficient utilizing the Bayesian hypothesis selection algorithm similar to [12] at the second step. The final step is projecting the estimated tire forces at the first step onto the tire model using the CKF, and feedback that information to the proposed TF-KF to substantially enhance the accuracy and robustness of the estimated tire forces.

A. Tire model

Before the proposed TFF-CKF, a brief summary of the tire model [15], [16] and the linearized tire model are provided in this subsection. The tire model is a function that is constructed with highly precise empirical data, and the tire model provides the longitudinal and lateral tire forces. To

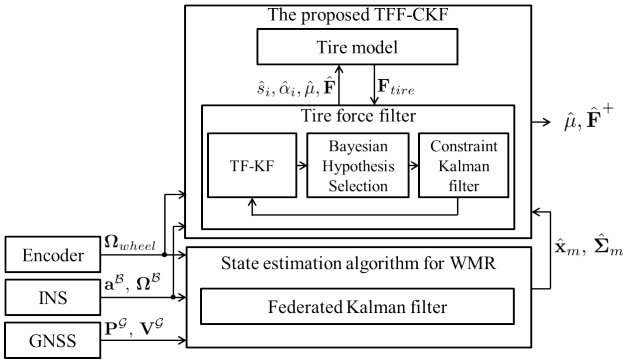

Fig. 2: A block diagram of the proposed TFF-CKF to estimate the tire forces and friction coefficients.

obtain the longitudinal and lateral tire forces from the tire model (e.g., $F^x_{i,tire}$ and $F^y_{i,tire}$, respectively), the vertical tire force F^z_i, slip ratio s_i, slip angle α_i, and friction coefficient μ are required according to the combined slip theory [22]. The vertical tire forces can be expressed with the accelerometer measurements using the effective mass approach [9], [18]. The bias compensated accelerometer measurements $\bar{\mathbf{a}}^{\mathcal{B}} (\in \Re^3) = \mathbf{a}^{\mathcal{B}} + \mathbf{g}^{\mathcal{B}} + \bar{\mathbf{\Omega}}^{\mathcal{B}} \times \hat{\mathbf{V}}^{\mathcal{B}} - \hat{\mathbf{b}}_a = [\bar{a}^x\ \bar{a}^y\ \bar{a}^z]^{\mathrm{T}}$ are used for the vertical tire forces estimation to improve the performance, where the bias compensated gyroscope measurements $\bar{\mathbf{\Omega}}^{\mathcal{B}} (\in \Re^3) = \mathbf{\Omega}^{\mathcal{B}} - \hat{\mathbf{b}}_\Omega$, $\hat{\mathbf{b}}_a \in \Re^3$ is the estimated accelerometer bias, and $\hat{\mathbf{b}}_\Omega \in \Re^3$ is the estimated gyroscope bias. The vertical forces are expressed as [18]

$$\begin{aligned}
\bar{F}^z_{\mathrm{lf}}(\bar{\mathbf{a}}^{\mathcal{B}}) &= m_{tot}\left(\frac{|r^x_{\mathrm{lr}}|}{|r^x_{\mathrm{lf}}|+|r^x_{\mathrm{lr}}|}\bar{a}^z - \frac{|r^z_{\mathrm{lf}}|}{|r^x_{\mathrm{lf}}|+|r^x_{\mathrm{lr}}|}\bar{a}^x\right) \\
&\quad \cdot \left(\frac{1}{2} - \frac{|r^z_{\mathrm{lf}}|}{|r^y_{\mathrm{rf}}|+|r^y_{\mathrm{lf}}|\bar{a}^z}\bar{a}^y\right), \qquad (4)\\
\bar{F}^z_{\mathrm{rf}}(\bar{\mathbf{a}}^{\mathcal{B}}) &= m_{tot}\left(\frac{|r^x_{\mathrm{rr}}|}{|r^x_{\mathrm{rr}}|+|r^x_{\mathrm{rf}}|}\bar{a}^z - \frac{|r^z_{\mathrm{rf}}|}{|r^x_{\mathrm{rf}}|+|r^x_{\mathrm{rr}}|}\bar{a}^x\right) \\
&\quad \cdot \left(\frac{1}{2} + \frac{|r^z_{\mathrm{rf}}|}{|r^y_{\mathrm{rf}}|+|r^y_{\mathrm{lf}}|\bar{a}^z}\bar{a}^y\right), \qquad (5)\\
\bar{F}^z_{\mathrm{lr}}(\bar{\mathbf{a}}^{\mathcal{B}}) &= m_{tot}\left(\frac{|r^x_{\mathrm{lf}}|}{|r^x_{\mathrm{lf}}|+|r^x_{\mathrm{lr}}|}\bar{a}^z + \frac{|r^z_{\mathrm{lr}}|}{|r^x_{\mathrm{lf}}|+|r^x_{\mathrm{lr}}|}\bar{a}^x\right) \\
&\quad \cdot \left(\frac{1}{2} - \frac{|r^z_{\mathrm{lr}}|}{|r^y_{\mathrm{lr}}|+|r^y_{\mathrm{rr}}|\bar{a}^z}\bar{a}^y\right), \qquad (6)\\
\bar{F}^z_{\mathrm{rr}}(\bar{\mathbf{a}}^{\mathcal{B}}) &= m_{tot}\left(\frac{|r^x_{\mathrm{rf}}|}{|r^x_{\mathrm{rf}}|+|r^x_{\mathrm{rr}}|}\bar{a}^z + \frac{|r^z_{\mathrm{rr}}|}{|r^x_{\mathrm{rf}}|+|r^x_{\mathrm{rr}}|}\bar{a}^x\right) \\
&\quad \cdot \left(\frac{1}{2} + \frac{|r^z_{\mathrm{rr}}|}{|r^y_{\mathrm{lr}}|+|r^y_{\mathrm{rr}}|\bar{a}^z}\bar{a}^y\right). \qquad (7)
\end{aligned}$$

The slip ratio and angle can be calculated using the estimated velocity of the WMR and measured velocity of each wheel $V_{O,i}$. The estimated slip ratio $\hat{s}_i$ and slip angle $\hat{\alpha}_i$ are defined as

$$\begin{aligned}
\hat{s}_i[k] &= \frac{V_{O,i}[k] - \left(\hat{V}^{\mathcal{B}}_x[k] + \Delta V^x_{O,i}[k]\right)}{\max\left(V_{O,i}[k], \hat{V}^{\mathcal{B}}_x[k] + \Delta V^x_{O,i}[k]\right)}, \qquad (8)\\
\hat{\alpha}_i[k] &= \tan^{-1}\left(\frac{\hat{V}^{\mathcal{B}}_y[k] + \Delta V^y_{O,i}[k]}{\max\left(V_{O,i}[k], \hat{V}^{\mathcal{B}}_x[k] + \Delta V^x_{O,i}[k]\right)}\right), \qquad (9)
\end{aligned}$$

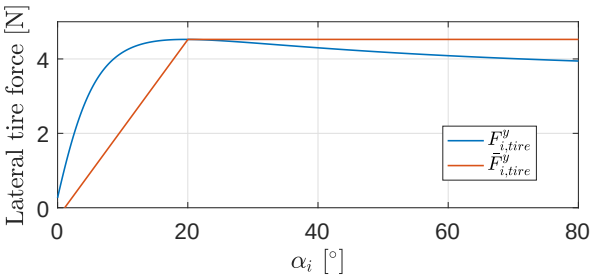

Fig. 3: The magic formula tire model and the linearized tire model for the lateral tire forces.

where $\hat{V}_x^{\mathcal{B}}$ and $\hat{V}_y^{\mathcal{B}}$ are the estimated longitudinal and lateral velocity of the WMR in $\{\mathcal{B}\}$ which can be obtained with the estimated velocity $\hat{\mathbf{V}}^{\mathcal{G}}$ using the FKF and the coordinate transformation matrix $\mathbf{C}_{\mathcal{G}}^{\mathcal{B}}$, i.e., $\hat{V}_x^{\mathcal{B}} = \mathbf{C}_{\mathcal{G}}^{\mathcal{B}}(1,:)\hat{\mathbf{V}}^{\mathcal{G}}$ and $\hat{V}_y^{\mathcal{B}} = \mathbf{C}_{\mathcal{G}}^{\mathcal{B}}(2,:)\hat{\mathbf{V}}^{\mathcal{G}}$. Note that the lever arm effect [23] is compensated for adding $\Delta V_{O,i}^x$ and $\Delta V_{O,i}^y$ from $\hat{V}_x^{\mathcal{B}}$ and $\hat{V}_y^{\mathcal{B}}$, respectively, in (8) and (9), where $[\Delta V_{O,i}^x\ \Delta V_{O,i}^y\ \Delta V_{O,i}^z]^{\mathrm{T}} = \bar{\mathbf{\Omega}}^{\mathcal{B}} \times \tilde{\mathbf{r}}_i^{\mathcal{B}}$ and the lever arm vector $\tilde{\mathbf{r}}_i^{\mathcal{B}} = [r_i^x\ r_i^y\ r_i^z + r_{eff}]^{\mathrm{T}}$. The friction coefficient is essential for the tire model, and it can be changed while driving. Therefore, we cannot obtain the tire forces using the tire model before the friction coefficient is estimated. Therefore, a linearized tire model is proposed to estimate the lateral tire force of each wheel without the friction coefficient. The linearized tire model for the lateral tire force $\bar{F}_{i,tire}^y$ is defined as

$$\bar{F}_{i,tire}^y = \mu \cdot \mathrm{sign}(\alpha_i) \cdot \min\left(\left| \frac{D_i + a_1}{\alpha_{max} + a_2} (\alpha_i + a_2) \right|, D_i + a_1 \right),$$

where D_i is the peak of the tire model which is a function of F_i^z, α_{max} is a slip angle that has the maximum tire force, and a_1 and a_2 are the offset parameters from the tire model. Fig. 3 shows the tire model and the linearized tire model. The sum of the lateral tire forces can be estimated as $m_{tot}\bar{a}^y$. To estimate the lateral tire force of each wheel, the sum of the lateral tire forces are distributed as

$$\bar{F}_i^y = \frac{\bar{F}_{i,tire}^y}{\sum_{j \in A} \bar{F}_{j,tire}^y} m_{tot} \bar{a}^y. \tag{10}$$

The friction coefficients in the denominator and nominator of (10) are canceled out, so we can estimate the lateral tire force of each wheel without the friction coefficient using the linearized tire model.

B. Tire Force Estimation

The tire force and torque vector $\mathbf{F} \in \Re^{14}$ of the WMR at the k-th time step is defined as $\mathbf{F}[k] = [F_{\mathrm{lf}}^x\ F_{\mathrm{rf}}^x\ F_{\mathrm{lr}}^x\ F_{\mathrm{rr}}^x\ F_{\mathrm{lf}}^y\ F_{\mathrm{rf}}^y\ F_{\mathrm{lr}}^y\ F_{\mathrm{rr}}^y\ F_{\mathrm{lf}}^z\ F_{\mathrm{rf}}^z\ F_{\mathrm{lr}}^z\ F_{\mathrm{rr}}^z\ \tau_{\mathrm{lr}}\ \tau_{\mathrm{rr}}]^{\mathrm{T}}$, where τ_i is the input torque of the i wheel. Note that torque inputs of the front wheels are not included in the tire force and torque vector, because the system is a RWD WMR as described in Section II. See Fig. 1 for the definitions of the tire forces and torque inputs. Using the fact that the tire forces increase or decrease continuously, the tire force and torque vector at time step $k+1$ can be approximated to $\mathbf{F}[k]$ when the time interval is small enough. With this approximation, we can express the system model equation for $\mathbf{F}$ similar to the random walk model in [9], [12] as

$$\mathbf{F}[k+1] = \mathbf{F}[k] + \mathbf{w}_F[k], \tag{11}$$

where $\mathbf{w}_F \sim \mathcal{N}(0, \mathbf{Q}_F)$ is the process noise which is related to the changed tire forces during the time step k to $k+1$. The CarSim simulation results in Sec. IV show that the system model equation in (11) works adequately for the proposed TFF-CKF. Then we can estimate the time propagation of $\mathbf{F}$ using the following equation.

$$\hat{\mathbf{F}}^-[k+1] = \hat{\mathbf{F}}[k].$$

As it is discussed in Section II, differentiated gyroscope measurements have large errors. Thus, we use (2) yet not (1) to found the measurement equation for the proposed TF-KF. The lateral and vertical tire forces of each wheel can be estimated using (10) and (4)-(7), respectively. The first column of (2) and (3) are used to estimate the longitudinal tire forces, and the torque inputs τ_{lr} and τ_{rr} are equal due to the differential gear attached to the both rear wheels. Consequently, the measurement equation for the tire force and torque vector at time step k is founded as

$$\begin{aligned} \mathbf{z}_F[k] &= \begin{bmatrix} m_{tot}\bar{a}^x[k] \\ \mathcal{I}_{wheel}\dot{\mathbf{\Omega}}_{wheel}[k] \\ [\bar{F}_{\mathrm{lf}}^y\ \bar{F}_{\mathrm{rf}}^y\ \bar{F}_{\mathrm{lr}}^y\ \bar{F}_{\mathrm{rr}}^y]^{\mathrm{T}} \\ [\bar{F}_{\mathrm{lf}}^z\ \bar{F}_{\mathrm{rf}}^z\ \bar{F}_{\mathrm{lr}}^z\ \bar{F}_{\mathrm{rr}}^z]^{\mathrm{T}} \\ 0 \end{bmatrix}, \\ &= \mathbf{H}_F\mathbf{F}[k] + \mathbf{v}_F[k], \end{aligned} \tag{12}$$

where

$$\begin{aligned} \mathbf{H}_F &= \begin{bmatrix} \mathbf{H}_{F,1} & \mathbf{H}_{F,2} & \mathbf{O}_{1\times4} & \mathbf{O}_{1\times2} \\ \mathbf{H}_{F,3} & \mathbf{O}_{4\times4} & \mathbf{O}_{4\times4} & \mathbf{H}_{F,4}^{\mathrm{T}} \\ \mathbf{H}_{F,5} & \mathbf{H}_{F,6} & \mathbf{O}_{4\times4} & \mathbf{O}_{4\times2} \\ \mathbf{O}_{4\times4} & \mathbf{O}_{4\times4} & \mathbf{I}_{4\times4} & \mathbf{O}_{4\times2} \\ \mathbf{O}_{1\times4} & \mathbf{O}_{1\times4} & \mathbf{O}_{1\times4} & \mathbf{H}_{F,7} \end{bmatrix}, \\ \mathbf{H}_{F,1} &= \begin{bmatrix} \cos\delta_{\mathrm{lf}} & \cos\delta_{\mathrm{rf}} & 1 & 1 \end{bmatrix}, \\ \mathbf{H}_{F,2} &= \begin{bmatrix} -\sin\delta_{\mathrm{lf}} & -\sin\delta_{\mathrm{rf}} & 0 & 0 \end{bmatrix}, \\ \mathbf{H}_{F,3} &= -r_{eff} \cdot I_{4\times4}, \\ \mathbf{H}_{F,4} &= \begin{bmatrix} \mathbf{O}_{2\times2} & \mathbf{I}_{2\times2} \end{bmatrix}, \\ \mathbf{H}_{F,5} &= \begin{bmatrix} \sin\delta_{\mathrm{lf}} & 0 & 0 & 0 \\ 0 & \sin\delta_{\mathrm{rf}} & 0 & 0 \\ 0 & 0 & 0 & 0 \\ 0 & 0 & 0 & 0 \end{bmatrix}, \\ \mathbf{H}_{F,6} &= \begin{bmatrix} \cos\delta_{\mathrm{lf}} & 0 & 0 & 0 \\ 0 & \cos\delta_{\mathrm{rf}} & 0 & 0 \\ 0 & 0 & 1 & 0 \\ 0 & 0 & 0 & 1 \end{bmatrix}, \\ \mathbf{H}_{F,7} &= \begin{bmatrix} 1 & -1 \end{bmatrix}, \end{aligned}$$

$\dot{\mathbf{\Omega}} = [\dot{\Omega}_{wheel,\mathrm{lf}}\ \dot{\Omega}_{wheel,\mathrm{rf}}\ \dot{\Omega}_{wheel,\mathrm{lr}}\ \dot{\Omega}_{wheel,\mathrm{rr}}]^{\mathrm{T}}$, $\mathbf{O}_{a\times b}$ is the zero matrix of size $[a \times b]$ and $\mathbf{I}_{a\times b}$ is the identity matrix of size $[a \times b]$. Exploiting the standard KF, the measurement update

of the tire force and torque vector is expressed as

$$\begin{aligned}
\hat{\mathbf{\Sigma}}_F^-[k] &= \hat{\mathbf{\Sigma}}_F[k-1] + \mathbf{Q}_F, &(14)\\
\mathbf{S}_F[k] &= \mathbf{H}_F \hat{\mathbf{\Sigma}}_F^-[k] \mathbf{H}_F^{\mathrm{T}} + \mathbf{R}_F,\\
\mathbf{K}_F[k] &= \hat{\mathbf{\Sigma}}_F^-[k] \mathbf{H}_F^{\mathrm{T}} \mathbf{S}_F^{-1}[k],\\
\hat{\mathbf{F}}[k] &= \hat{\mathbf{F}}^-[k] + \mathbf{K}_F[k](\mathbf{z}_F[k] - \mathbf{H}_F \hat{\mathbf{F}}^-[k]), &(15)\\
\hat{\mathbf{\Sigma}}_F[k] &= (\mathbf{I}_{14\times14} - \mathbf{K}_F[k]\mathbf{H}_F)\hat{\mathbf{\Sigma}}_F^-[k], &(16)
\end{aligned}$$

where $\hat{\mathbf{\Sigma}}_F^- \in \Re^{14\times14}$, $\mathbf{S}_F \in \Re^{16\times16}$, $\mathbf{K}_F \in \Re^{14\times16}$, $\hat{\mathbf{F}} \in \Re^{14}$, and $\hat{\mathbf{\Sigma}}_F \in \Re^{14\times14}$ are the error covariance of the time propagated tire force and torque vector, the error covariance of the tire force and torque residual, the tire force Kalman gain, the estimated tire force and torque vector, and the error covariance of the estimated tire force and torque vector, respectively. The covariance of the measurement noise $\mathbf{R}_F$ is calculated by using the Taylor series of the measurement equations in (12). The estimated tire force and torque vector $\hat{\mathbf{F}}$ provides the estimated tire forces of each wheel, i.e., $\hat{F}_i^x$, $\hat{F}_i^y$, and $\hat{F}_i^z$, and $\hat{\mathbf{F}}$ is used to estimate the friction coefficient in the next subsection.

C. Friction Coefficient Estimation

Typically, the magnitude of the friction coefficient is between 0.1 and 1.1, i.e., 0.2 for the ice, 0.5-0.7 for the wet concrete, and 0.8-1 for the dry asphalt/concrete [24]. Using this property of the friction coefficient, the n-th candidate of the friction coefficient μ_n can be defined between 0.1 to 1.1, and then the conditional probability $\Pr\left(\mu_n|\hat{\mathbf{F}}^{x,y}\right)$ with $\hat{F}_i^x$, $\hat{F}_i^y$, and $\hat{F}_i^z$ is expressed as

$$\Pr(\mu_n|\hat{\mathbf{F}}^{x,y}[k]) = \frac{p\left(\hat{\mathbf{F}}^{x,y}[k]|\mu_n\right)\Pr\left(\mu_n|\hat{\mathbf{F}}^{x,y}[k\text{–}1]\right)}{\sum_{n=1}^{N} p\left(\hat{\mathbf{F}}^{x,y}[k]|\mu_n\right)\Pr\left(\mu_n|\hat{\mathbf{F}}^{x,y}[k\text{–}1]\right)}, \quad (17)$$

where

$$\begin{aligned}
\hat{\mathbf{F}}^{x,y} &= [\hat{F}_{\mathrm{lf}}^x\ \hat{F}_{\mathrm{rf}}^x\ \hat{F}_{\mathrm{lr}}^x\ \hat{F}_{\mathrm{rr}}^x\ \hat{F}_{\mathrm{lf}}^y\ \hat{F}_{\mathrm{rf}}^y\ \hat{F}_{\mathrm{lr}}^y\ \hat{F}_{\mathrm{rr}}^y]^{\mathrm{T}},\\
p\left(\hat{\mathbf{F}}^{x,y}[k]|\mu_n\right) &= p\left(\hat{\mathbf{F}}^{x,y}[k]|\mathbf{F}_{tire}(\hat{s}_i[k], \hat{\alpha}_i[k], \hat{F}_i^z[k], \mu_n)\right)\\
&= e^{-(\hat{\mathbf{F}}^{x,y}[k] - \mathbf{F}_{tire}[k])^{\mathrm{T}} \hat{\Sigma}_{\mathbf{F}^{x,y}}^{-1} (\hat{\mathbf{F}}^{x,y}[k] - \mathbf{F}_{tire}[k])/2}/\lambda, \quad (18)\\
\hat{\Sigma}_{\mathbf{F}^{x,y}} &= \hat{\Sigma}_{\mathbf{F}}(1\text{:}8, 1\text{:}8),
\end{aligned}$$

where N is the number of the candidates and λ is the normalization factor. The expression (17) and (18) are derived using the Bayesian rule [12]. Different from the Bayesian hypothesis selection algorithm in [12], we give weights inverse proportional to the estimated error covariances of the longitudinal and lateral tire forces while calculating the likelihood $p\left(\hat{\mathbf{F}}^{x,y}[k]|\mu_n\right)$ as expressed in (18). With $\Pr(\mu_n|\hat{\mathbf{F}}^{x,y})$, the estimated friction coefficient $\hat{\mu}$ at the time step k is expressed as [12]

$$\hat{\mu}[k] = \sum_{n=1}^{N} \Pr\left(\mu_n|\hat{\mathbf{F}}^{x,y}[k]\right)\mu_n.$$

D. Tire Force Update and Feedback Using Tire Model

The estimated tire forces using the proposed TF-KF contains errors due to the effective mass approach and the linearized tire model. To compensate these errors, the tire model and estimated friction coefficient are used in this subsection. The tire model provides highly precise empirical data, so the estimated tire forces $\hat{\mathbf{F}}$ should satisfy the following constraints $\mathbf{d}$ which is founded using the tire model.

$$\mathbf{d}[k] = \mathbf{D}\mathbf{F}[k] + \mathbf{v}_D, \quad (19)$$

where

$$\mathbf{d}[k] = \begin{bmatrix}
F_{\mathrm{lf},tire}^x(\hat{s}_{\mathrm{lf}}[k], \hat{\alpha}_{\mathrm{lf}}[k], \hat{F}_{\mathrm{lf}}^z[k], \hat{\mu}[k])\\
F_{\mathrm{rf},tire}^x(\hat{s}_{\mathrm{rf}}[k], \hat{\alpha}_{\mathrm{rf}}[k], \hat{F}_{\mathrm{rf}}^z[k], \hat{\mu}[k])\\
F_{\mathrm{lr},tire}^x(\hat{s}_{\mathrm{lr}}[k], \hat{\alpha}_{\mathrm{lr}}[k], \hat{F}_{\mathrm{lr}}^z[k], \hat{\mu}[k])\\
F_{\mathrm{rr},tire}^x(\hat{s}_{\mathrm{rr}}[k], \hat{\alpha}_{\mathrm{rr}}[k], \hat{F}_{\mathrm{rr}}^z[k], \hat{\mu}[k])\\
F_{\mathrm{lf},tire}^y(\hat{s}_{\mathrm{lf}}[k], \hat{\alpha}_{\mathrm{lf}}[k], \hat{F}_{\mathrm{lf}}^z[k], \hat{\mu}[k])\\
F_{\mathrm{rf},tire}^y(\hat{s}_{\mathrm{rf}}[k], \hat{\alpha}_{\mathrm{rf}}[k], \hat{F}_{\mathrm{rf}}^z[k], \hat{\mu}[k])\\
F_{\mathrm{lr},tire}^y(\hat{s}_{\mathrm{lr}}[k], \hat{\alpha}_{\mathrm{lr}}[k], \hat{F}_{\mathrm{lr}}^z[k], \hat{\mu}[k])\\
F_{\mathrm{rr},tire}^y(\hat{s}_{\mathrm{rr}}[k], \hat{\alpha}_{\mathrm{rr}}[k], \hat{F}_{\mathrm{rr}}^z[k], \hat{\mu}[k])
\end{bmatrix},$$

$$\mathbf{D} = \begin{bmatrix} \mathbf{I}_{8\times8} & \mathbf{O}_{6\times6} \end{bmatrix},$$

and $\mathbf{v}_D \sim \mathcal{N}(0, \mathbf{R}_D)$ is the constraint noise which is generated due to the noises in $\hat{s}_i$, $\hat{\alpha}_i$, $\hat{F}_i^z$, $\hat{\mu}$. The constraints in (19) do not have the information of the vertical tire forces. Yet, the constraints of the vertical tire forces are not essential, because the vertical tire forces can be obtained from $\hat{\mathbf{F}}$. Then the updated tire force and torque vector $\hat{\mathbf{F}}^+$ and the error covariance of $\hat{\mathbf{\Sigma}}_F^+$ using the CKF is

$$\begin{aligned}
\mathbf{K}_F^+[k] &= \hat{\mathbf{\Sigma}}_F[k]\mathbf{D}^{\mathrm{T}}\left(\mathbf{D}\hat{\mathbf{\Sigma}}_F[k]\mathbf{D}^{\mathrm{T}} + \mathbf{R}_D[k]\right)^{-1},\\
\hat{\mathbf{F}}^+[k] &= \hat{\mathbf{F}}[k] - \mathbf{K}_F^+\left(\mathbf{D}\hat{\mathbf{F}}[k] - \mathbf{d}[k]\right), &(20)\\
\hat{\mathbf{\Sigma}}_F^+[k] &= (\mathbf{I}_{14\times14} - \mathbf{K}_F^+[k]\mathbf{D})\hat{\mathbf{\Sigma}}_F[k], &(21)
\end{aligned}$$

where $\hat{\mathbf{\Sigma}}_F$ is the error covariance of the estimated tire force and torque vector. The updated tire force and torque vector $\hat{\mathbf{F}}^+$ is the projection of $\hat{\mathbf{F}}$ onto the tire model based constraints in (19), and the expression (20) and (21) are derived to estimate the tire force and torque vector with minimum mean square error (MMSE). To estimate $\mathbf{R}_D = \mathrm{diag}([R_{D,1}\ R_{D,2}\ R_{D,3}\ R_{D,4}])$, the variances of $\hat{s}_i$, $\hat{\alpha}_i$, $\hat{F}_i^z$, and $\hat{\mu}$ are required. The variance of $\hat{F}_i^z$ can be obtained using $\hat{\mathbf{\Sigma}}_F$, and it is clear that the probability density function $\Pr(\mu_n|\hat{\mathbf{F}}^{x,y})$ can be used to estimate the variance of $\hat{\mu}$. However, estimating the variances of $\hat{s}_i$ and $\hat{\alpha}_i$ are difficult, because the equations for $\hat{s}_i$ and $\hat{\alpha}_i$ are highly non-linear as expressed in (8) and (9). Therefore, we use the unscented transformation (UT) [25] with the estimated error covariance of the velocity in (16) and the covariance of the gyroscope measurement noise to calculate the variances of $\hat{s}_i$ and $\hat{\alpha}_i$. With the variances of $\hat{s}_i$, $\hat{\alpha}_i$, $\hat{F}_i^z$, and $\hat{\mu}$, which are, respectively, $\hat{\sigma}_{s,i}^2$, $\hat{\sigma}_{\alpha,i}^2$, $\hat{\sigma}_{z,i}^2$, and $\hat{\sigma}_{\mu}^2$, we can use the UT to estimate $\mathbf{R}_D$. Note that the estimation errors due to the effective mass approach and the linearized tire model in $\hat{\mathbf{F}}$ can be reduced using the proposed TFF-CKF, because the

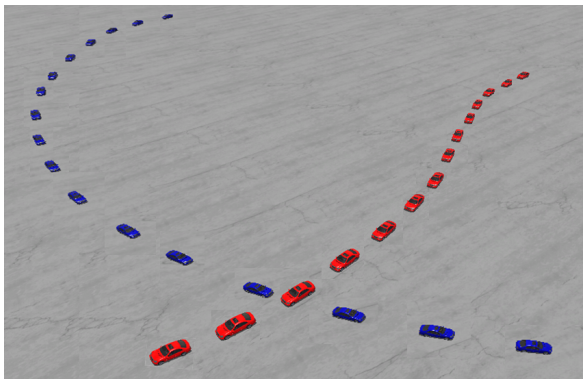

Fig. 4: Examples of the simulated trajectories in CarSim. Blue and red car follow circular and S shape trajectories, respectively

proposed TFF-CKF optimally projects $\hat{\mathbf{F}}$ onto the tire model using the error covariance of $\hat{\mathbf{F}}$ and the uncertainty of the tire model $\mathbf{R}_D$. As it is depicted in Fig. 2, the proposed TFF-CKF feedback the estimation results of the CKF to the proposed TF-KF, so the time propagation of the tire force and torque vector can be estimated by substituting $\hat{\mathbf{F}}^+$ and $\hat{\mathbf{\Sigma}}_F^+$ instead of $\hat{\mathbf{F}}$ and $\hat{\mathbf{\Sigma}}_F$ in (12) and (14), respectively. The estimation accuracy of the tire forces and friction coefficients can be improved when the updated tire force and torque vector is used for the time propagation. With the updated tire force and torque vector $\hat{\mathbf{F}}^+[k]$, more accurate $\hat{\mathbf{F}}^-[k+1]$ and $\hat{\mathbf{F}}[k+1]$ can be obtained utilizing (12) and (15), respectively. The estimation performance of the friction coefficients is also closely related to this accuracy of $\hat{\mathbf{F}}[k+1]$. Therefore, we can obtain more accurate friction coefficient with the updated tire force and torque vector. See Section IV for the estimation results of the tire forces and friction coefficients using the proposed TFF-CKF.

IV. SIMULATION AND EXPERIMENT RESULTS

In this section, simulation and experiment results of the proposed TFF-CKF are provided. For the simulation, the CarSim software which is widely used in the vehicular area and also for high-speed WMRs is used to generate the true tire forces and torques and sensor measurements. A RWD WMR which has the same sensor configuration in Fig. 1 is implemented for experiments, and the real sensor data from the implemented RWD WMR is used to verify the proposed TFF-CKF. The simulation and experiment results are described in Sec. IV-A and IV-B, respectively.

A. CarSim Simulations

The D-class Sedan vehicle model which is provided in the CarSim software is selected and modified as a RWD WMR in Section II. The sprung mass and unsprung mass of the van are, respectively, 1370Kg and 160Kg, and the roll, pitch, and yaw inertia of the sprung mass are, respectively, 671.3Kg·m^2, 1972.8Kg·m^2, and 2315.3Kg·m^2. The WMR considered in this paper do not have suspensions, so we use suspensions with high stiffnesses (e.g., 385N/mm for each suspension) to reduce their effects. The measurement noise covariance matrices are defined based on the specifications of the real

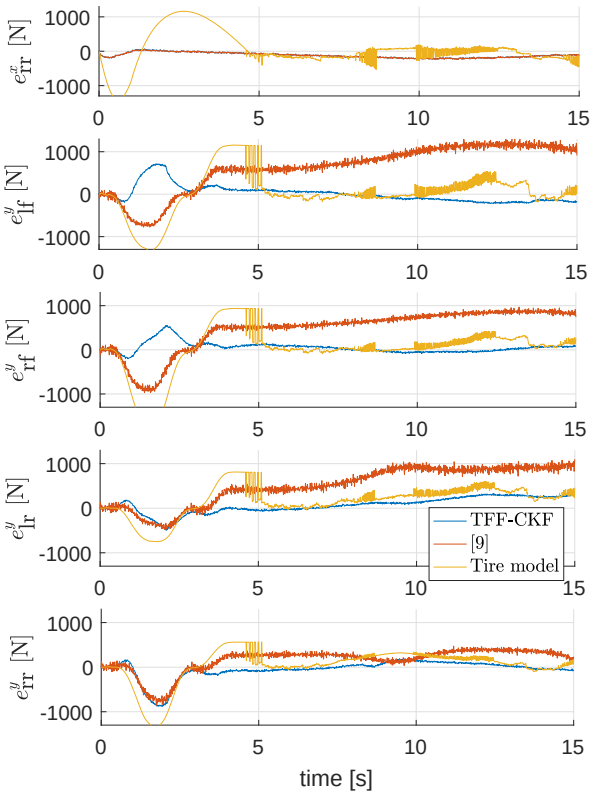

Fig. 5: Estimation errors of the longitudinal and lateral tire forces.

onboard sensors. For the INS and GNSS measurements, the specifications of the Advanced Navigation Spatial is used. An encoder implemented at each wheel generates 1024 pulses per revolution to measure the angular velocity of the wheel, and the standard deviation of the encoder measurement noise is assumed as 10 pulses per second.

The conventional PID controller is employed to generate the steering angle and torque inputs with the current velocity and yaw rate of the WMR. The gains of the PID controller are empirically selected based on the simulations with various desired trajectories generated to have circular or S shape as shown in Fig. 4. A plain concrete road with the friction coefficient $\mu = 1$ is used to verify the estimation performance of the proposed TFF-CKF. To apply the effect of the modeling uncertainty, modeling errors with 0.5%×(true value) standard deviation are added to the mass, moment of inertia, and position of the CoG and wheels. The performance of the proposed TFF-CKF is analyzed using 264 number of simulations.

To evaluate the tire force estimation performances of the proposed TFF-KF, the estimation errors of the longitudinal and lateral tire forces (e.g., $e_i^x = \hat{F}_i^{x,+} - F_i^x$ and $e_i^y = \hat{F}_i^{y,+} - F_i^y$, respectively) are calculated using the true tire forces in $\{\mathcal{B}\}$, F_i^x, F_i^y, and F_i^z, from the CarSim software. The CKF of the proposed TFF-CKF is used after the error covariance of the estimated velocity is converged (e.g., after 3.2s), because the estimated slip ratio and angle have large errors before the estimated velocity of the WMR is converged.

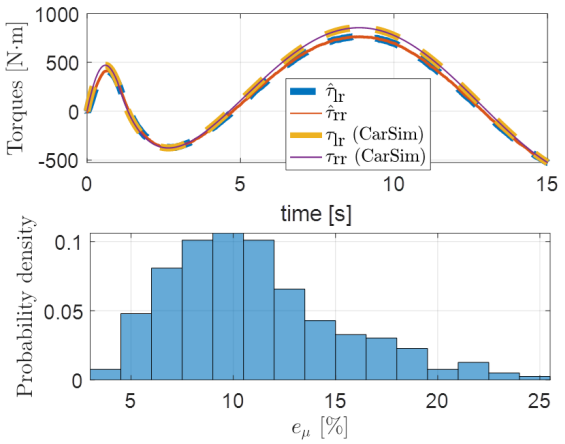

Fig. 6: Estimated torque inputs and histogram of the estimated friction coefficient errors.

Fig. 5 shows an example of the longitudinal and lateral tire force estimation errors, and the estimated tire forces using the proposed TFF-CKF has the best performance after the friction coefficient is converged (e.g., after 5.5s). One of the recent existing tire force estimation algorithm [9] estimates the front and rear lateral tire forces using the 3-DOF bicycle model, and the estimated front and rear lateral tire forces of the 3-DOF bicycle model are distributed using weights which are proportional to the estimated vertical tire forces. The lateral tire force estimation performance of the proposed TFF-CKF is better than the tire force estimation algorithm in [9], because the proposed TFF-CKF does not use only the estimated vertical tire forces yet also the estimated slip angles as expressed in (10). The tire model has errors due to the estimation errors of the slip ratio, slip angle, vertical tire force, and friction coefficient as shown in Fig. 5, yet the proposed TFF-CKF adequately combine the information of the estimated tire forces using the proposed TF-KF and the tire model.

The estimated and true rear torques are shown in Fig. 6, and the estimated torques shows that the proposed TFF-CKF adequately estimate the torque inputs. The friction coefficients are estimated using the proposed TFF-CKF after the error covariance of the estimated velocity is converged (e.g., after 3.2s), and the initial guesses of the friction coefficients are randomly generated to have the uniform distribution on the interval $[0.85,\ 1.15]$. The candidates of the friction coefficient are selected from 0.1 to 1.1 with the interval 0.05. To evaluate the friction coefficient estimation performance of the proposed TFF-CKF, the root mean square error (RMSE) of the estimated friction coefficient is defined as $e_\mu = 100 \times \sqrt{\frac{\sum_{\gamma=1}^{\Gamma}\{(\hat{\mu}(\gamma)-\mu(\gamma))/\mu(\gamma)\}^2}{\Gamma}}$, where γ represent the γ-th element of μ (or $\hat{\mu}$), and Γ is the length of μ (or $\hat{\mu}$). The RMSE of the estimated friction coefficient using the proposed TFF-CKF is calculated, and the mean $\bar{e}_\mu$ and standard deviation σ_{e_μ} of the RMSE are 11.04% and 4.24%, respectively. The histogram of e_μ in Fig. 6 shows that e_μ are less than 15% for 82.96% of 264 simulations.

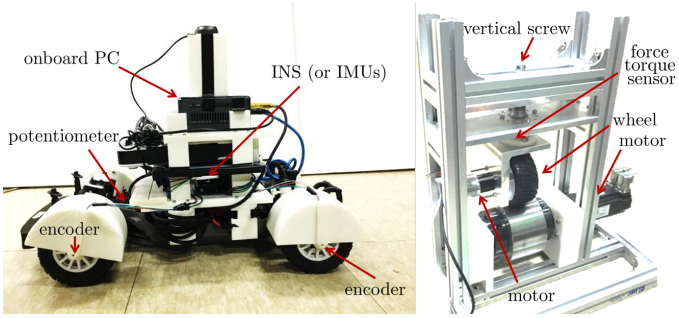

Fig. 7: Implemented RWD WMR with onboard sensors and tire model measuring equipment.

B. Outdoor Experiments

The implemented RWD WMR using the traxxas Rally 1/10 RC car is shown in Fig. 7. An Advanced Navigation Spatial INS and GNSS receiver, four RLS RM08 encoders, Intel NUC onboard PC, and a Piher PT-10 potentiometer are used for the implemented RWD WMR. The potentiometer measures the rotated angle of a servo motor which steers the front wheels, and the relations between the steering angle of the front wheels and the rotated angle of the servo motor are measured using the motion capture system OptiTrack. Fig. 7 also shows the implemented tire model measuring equipment. The tire model measuring equipment is designed to measure the longitudinal and lateral tire forces of the wheel when the slip ratio, slip angle, and vertical force are given. By rotating a vertical screw at the top of the tire model measuring equipment, the vertical tire force of the wheel can be controlled. A Robotous RFT40-SA01 force-torque sensor measures the tire forces, and the tire model parameters are estimated using the measured tire forces.

The implemented RWD WMR which is controlled by a remote controller turns to left for seven times, and Fig. 8 shows the estimated tire forces and torque inputs using the proposed TFF-CKF. During the left turn, the longitudinal tire forces of the rear wheels, lateral tire forces, and vertical tire forces of the right wheels have peaks as shown in Fig. 8. The estimated longitudinal tire forces of the front wheels are approximately zero, because the front wheels do not have any actuator. The estimated friction coefficients for three different trajectories using the proposed TFF-CKF are shown in Fig. 9. For the three experiments (e.g., experiment 1, 2, and 3), the implemented RWD WMR drives on the same asphalt road, and the friction coefficients are calculated after all the wheel velocities reach 0.05m/s. The mean and standard deviation of the estimated friction coefficients are, respectively, $\bar{\mu} = 0.856$ and $\bar{\sigma}_\mu = 0.1071$, where the friction coefficient of the dry asphalt is 0.8-1 [24]. The simulation time for the 76.4s trajectory is about 26.16s using the MATLAB.

V. CONCLUSIONS

A novel real-time algorithm to estimate the full three-dimensional tire forces and friction coefficient, which is the proposed TFF-CKF, is proposed in this paper. The proposed TFF-CKF estimates the tire forces and friction coefficient of a car-like RWD four wheel WMR based on the

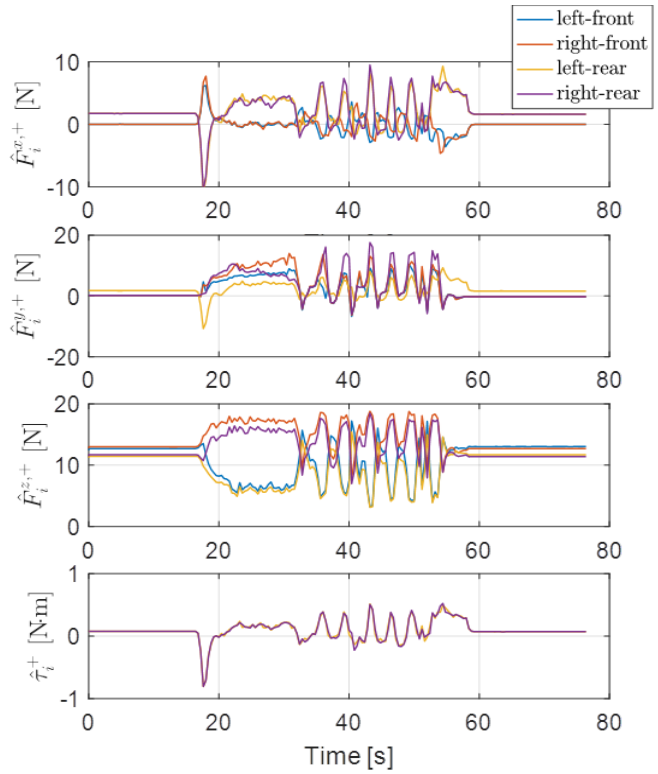

Fig. 8: Estimated tire forces and torque inputs using the proposed TFF-CKF.

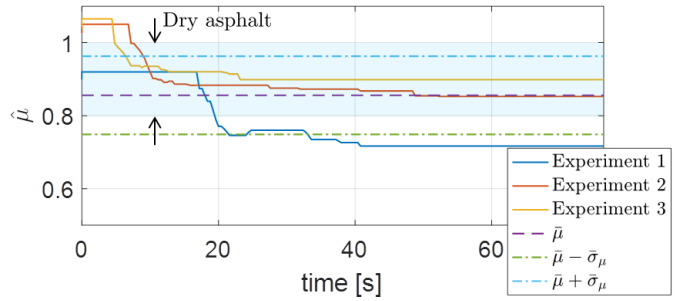

Fig. 9: Estimated friction coefficient of an asphalt road.

onboard sensors (e.g., onboard navigation sensors and wheel encoders) utilizing the tire model based constrained KF (CKF). Thanks to the feedback correction loop, the proposed TFF-CKF has advantages of accuracy and robustness. The proposed TFF-CKF can be used for the safety controls such as yaw stability control, traction control, and rollover prevention control. Our future work is incorporating the rotation dynamics to improve the accuracy of the estimated tire forces and formulating the vertical tire forces based on the dynamic equations of the WMRs.

REFERENCES

[1] W. Li, L. Ding, H. Gao, and M. Tavakoli. Haptic tele-driving of wheeled mobile robots under nonideal wheel rolling, kinematic control and communication time delay. *IEEE Trans. on Systems, Man, and Cybernetics: Systems*, 2017. Online Available: `http://ieeexplore.ieee.org/abstract/document/8017409/`.

[2] D. Chwa. Robust distance-based tracking control of wheeled mobile robots using vision sensors in the presence of kinematic disturbances. *IEEE Trans. on Industrial Electronics*, 63(10):6172–6183, 2016.

[3] R. Y. Hindiyeh and J. C. Gerdes. A controller framework for autonomous drifting: design, stability, and experimental validation. *Journal of Dynamic Systems, Measurement, and Control*, 136(3):051015–1–051015–9, Jun. 2014.

[4] G. Williams, N. Wagener, B. Goldfain, P. Drews, J. M. Rehg, B. Boots, and E. A. Theodorou. Information theoretic mpc for model-based reinforcement learning. In *Proc. IEEE Int'l Conf. on Robotics and Automation (ICRA)*, pages 1714–1721, 2017.

[5] M. Cutler, T. J. Walsh, and J. P. How. Real-world reinforcement learning via multifidelity simulators. *IEEE Trans. on Robotics*, 31(3):655–671, Jun. 2015.

[6] J. Yoon, J.-H. Oh, J.-H. Park, S. Kim, and D. Lee. Autonomous dynamic driving control of wheeled mobile robots. In *Proc. IEEE Int'l Conf. on Robotics and Automation (ICRA)*, pages 5274–5279, 2014.

[7] H. Yang, S.-Y. Jeon, and D. Lee. Fast zmp and friction force calculation of mobile robot trajectory on uneven trajectory. In *Proc. Inter'l Conf. on Ubiquitous Robots and Ambient Intelligence (URAI)*, pages 884–885, 2017.

[8] N. Seegmiller and A. Kelly. High-fidelity yet fast dynamic models of wheeled mobile robots. *IEEE Trans. on Robotics*, 32(3):614–625, May 2016.

[9] A. Rezaeian, R. Zarringhalam, S. Fallah, W. Melek, A. Khajepour, S.-K. Chen, N. Moshchuck, and B. Litkouhi. Novel tire force estimation strategy for real-time implementation on vehicle applications. *IEEE Trans. on Vehicular Technology*, 64(6):2231–2241, Jun. 2015.

[10] M. Doumiati, A. C. Victorino, and A. Charara. Onboard real-time estimation of vehicle lateral tire-road forces and sideslip angle. *IEEE Trans. on Mechatronics*, 16(4):601–614, Aug. 2011.

[11] D. A. Aligia, G. A. Magallan, and C. H. De Angelo. Ev traction control based on nonlinear observers considering longitudinal and lateral tire forces. *IEEE Trans. on Intelligent Transportation Systems*, 2017. Online Available: `http://ieeexplore.ieee.org/abstract/document/8082115/`.

[12] R. Rajamani, N. Piyabongkarn, J. Lew, K. Yi, and G. Phanomchoeng. Tire-road friction-coefficient estimation. *IEEE Control Systems Magazine*, 30(4):54–69, Aug. 2010.

[13] M. Acosta, A. Alatorre, S. Kanarachos, A. Victorino, and A. Charara. Estimation of tire forces, road grade, and road bank angle using tire model-less approaches and fuzzy logic. *Int'l Federation of Automatic Control*, 50(1):14836–14842, Jul. 2017.

[14] R. Rajamani, G. Phanomchoeng, D. Piyabongkarn, and J. Y. Lew. Algorithms for real-time estimation of individual wheel tire-road friction coefficients. *IEEE Trans. on Mechatronics*, 17(6):1183–1195, Dec. 2012.

[15] H. B. Pacejka and I. Besselink. Tire and vehicle dynamics 3rd ed. *Butterworth-Heinemann, London*, 2012.

[16] R. Rajamani. Vehicle dynamics and control 2nd ed. *Springer, New York*, 2006.

[17] D. Simon and T. Chia. Kalman filtering with state equality constraints. *IEEE Trans. on Aerospace and Electronic Systems*, 38(1):128–136, Aug. 2002.

[18] M. Doumiati, A. Victorino, A. Charara, and D. Lechner. Lateral load transfer and normal forces estimation for vehicle safety: Experimental evaluation. *Vehicle System Dynamics*, 47(12):1511–1533, Dec. 2009.

[19] N. A. Carlson. Federated square root filter for decentralized parallel processors. *IEEE Trans. on Aerospace and Electronic Systems*, 26(3):517–525, May 1990.

[20] K. Kim, S.-H. Kong, and S.-Y. Jeon. Slip and slide detection and adaptive information sharing algorithms for high-speed train navigation systems. *IEEE Trans. on Intelligent Transportation Systems*, 16(6):3193–3203, Jun. 2015.

[21] S. Merhav. Aerospace sensor systems and applications. *Springer, New York*, 2012.

[22] E. Bakker, H.B. Pacejka, and L. Linder. A new tire model with an application in vehicle dynamics studies. In *Proc. Autotechnologies Conference and Exposition*, pages 83–95, 1989.

[23] J. Seo, H. Lee, J. Lee, and C. Park. Lateral load transfer and normal forces estimation for vehicle safety: Experimental evaluation. *Int'l Journal of Control, Automation, and Systems*, 4(2):247–254, Apr. 2006.

[24] J. Y. Wong. Theory of ground vehicles 4th ed. *Wiley, New York*, 2008.

[25] D. Simon. Optimal state estimation. *Wiley, New York*, 2006.